molbank

MDPI

Communication

Microwave Assisted Synthesis, Crystal Structure and Hirshfeld Surface Analysis of Some 2-Formimidate-3-carbonitrile Derivatives Bearing 4H-Pyran and Dihydropyridine Moieties

Sizwe J. Zamisa * and Bernard Omondi

School of Chemistry and Physics, University of KwaZulu-Natal, Private Bag X54001, Durban 4000, South Africa; owaga@ukzn.ac.za

* Correspondence: zamisas@ukzn.ac.za

Abstract: Two 4H-pyran- and four dihydropyridine-based 2-formimidate-3-carbonitrile derivatives were synthesized via the conventional solvothermal and microwave radiation methods. The use of the latter technique led to the formation of the desired products in the order of minutes as compared to the former. The formation of the 2-formimidate-3-carbonitrile derivatives was confirmed using spectroscopic techniques whilst the molecular geometry and intermolecular interactions were investigated using single-crystal X-ray diffraction. The formimidate functional group was found to adopt an *E* configuration in all compounds and this coincides with those of closely related compounds on the Cambridge Structural Database (CSD). Classical but weak intermolecular C—H…O, C—H…N and C—H…π hydrogen bonds were observed in the crystal lattice. According to the Hirshfeld surface analysis, the C—H…π hydrogen bonds contributed the most towards the Hirshfeld surface (14.3–23.9%) than the other two hydrogen bonding types (9.6–12.7%).

Keywords: intermolecular contacts; triethylorthoformate; 2-amino-3-carbonitrile derivatives

Citation: Zamisa, S.J.; Omondi, B. Microwave Assisted Synthesis, Crystal Structure and Hirshfeld Surface Analysis of Some 2-Formimidate-3-carbonitrile Derivatives Bearing 4H-Pyran and Dihydropyridine Moieties. *Molbank* **2022**, *2022*, M1364. https://doi.org/10.3390/M1364

Academic Editor: Kristof Van Hecke

Received: 17 March 2022
Accepted: 4 May 2022
Published: 16 May 2022

1. Introduction

Compounds that contain 2-formimidate-3-carbonitrile moieties have gained attention in the synthesis of biologically active heterocycles, i.e., fused pyrimidines. The medicinal potency and function of fused pyrimidines can be tweaked by varying the nature of the ring that is adjoined to the pyrimidine [1]. For instance, 4H-pyran-fused pyrimidines have recently been used as potential antimicrobial [2–4], antiproliferative [5] and anticancer [6] agents whilst dihydropyridine-fused pyrimidines exhibit antidiabetic [7] and antioxidant [8] properties, amongst others. Although fused pyrimidines can be synthesized using precursors containing 2-formimidate-3-carbonitrile moieties, it is worth mentioning that they can also be formed using compounds bearing 2-formamidine-3-carbonitrile [2]. Using the former and latter precursors leads to the formation of ethanol [9] and dimethylamine [10] as by-products, respectively. Since ethanol is more environmentally friendly than dimethylamine, the use of 2-formimidate-3-carbonitrile precursors is ideal.

The conventional method of synthesizing 2-formimidate-3-carbonitrile derivatives involves a solvothermal reaction of the corresponding 2-amino-carbonitrile precursor and triethyl orthoformate in the presence of a suitable catalyst. Though the desired product is often isolated in good yields, the reaction times are often in the order of hours [11–23]. Thus, there is a need to explore other synthetic protocols that can significantly reduce the reaction times without compromising the reaction yields. Since these compounds are intermediates in the synthetic route of fused pyrimidines, there are very few structure-related reports on them.

In this work, we report the microwave-assisted synthesis of some novel 4H-pyran- and dihydropyridine-bearing 2-formimidate-3-carbonitrile derivatives. We hypothesize that using microwave radiation will lead to shorter reaction times whilst maintaining or

improving the reaction yields. We also investigated their preferred molecular geometry and the intermolecular interactions in the solid-state using single-crystal X-ray diffraction. The intermolecular interactions were further studied using Hirshfeld surface analysis.

2. Materials and Methods

All chemicals used in the syntheses of target molecules were of reagent grade purchased from commercial sources. These included: 2-fluorobenzaldehyde, 9-anthracenecarboxaldehyde, benzaldehyde, malonitrile, dimedone, ethanol, methanol, triethyl orthoformate, acetic acid, 4-bromoaniline, 4-methylaniline, and aniline. DMSO-d_6 was used as a solvent in solution NMR studies. ^{1}H- and ^{13}C-NMR spectra were recorded on a BRUKER 400 MHz (Karlsruh, German) spectrometer at room temperature and were referenced internally using the chosen deuterated solvent (see Supplementary Materials Figures S1–S12). Infrared spectra were recorded using a PerkinElmer (Waltham, MA, USA) spectrum 100 FT-IR spectrometer, and the data are reported as percentage transmittances from 4000 cm^{-1} to 400 cm^{-1} (see Supplementary Materials Figures S13–S17). Microwave reactions were carried out using a CEM Discover system. All reactions were performed in 30 mL pressurized vials fitted with "snap-on" caps. The 2-amino-4-(aryl)-7,7-dimethyl-5-oxo-5,6,7,8-tetrahydro-4*H*-chromene-3-carbonitrile (**i-a** and **i-b**) and 2-amino-1-phenyl-7,7-dimethyl-5-oxo-4-(aryl)-1,4,5,6,7,8-hexahydroquinoline-3-carbonitrile (**i-c** to **i-f**) precursors were synthesized using a modified procedure from the literature [24]. A Thermo-Scientific Flash 2000 was used to determine the elemental composition, and the melting-point determination was carried out using the Stuart Scientific SMP3 (Staffordshire, United Kingdom) melting-point apparatus.

*2.1. General Procedure for the Conventional Solvothermal Synthesis of 2-Formimidate-3-carbonitrile Derivatives (***ii-a** *to* **ii-f***)*

Triethyl orthoformate (20 mL), acetic acid (1 mL) and the corresponding 2-amino-3-carbonitrile precursor (2 mmol) were added to a 50 mL round bottom flask. The mixture was refluxed, and the reaction was monitored using TLC. Initially, the mixture had a very pale yellow colour, which gradually turned to dark red over the course of eight hours. The mixture was then left open overnight in the fume hood to allow evaporation of the excess triethyl orthoformate. The pure product was obtained by hot recrystallization using ethanol, filtered and dried under vacuum.

*2.2. General Procedure for the Microwave Synthesis of 2-Formimidate-3-carbonitrile Derivatives (***ii-a** *to* **ii-f***)*

Triethyl orthoformate (20 mL), acetic acid (1 mL) and the corresponding 2-amino-3-carbonitrile precursor (2 mmol) were added to a sealed 30 mL pressurized vial. The mixture was irradiated at 120 W in a single-mode microwave synthesis system. The reaction temperature was set at 150 °C for a duration of 20 min. The color of the mixture changed from colorless to dark red, signifying the completion of the reaction (confirmed via TLC). The mixture was then left open overnight in the fume hood to allow evaporation of the excess triethyl orthoformate. The pure product was obtained by hot recrystallization using ethanol, filtered and dried under vacuum.

2.2.1. Ethyl (*E*)-*N*-(3-Cyano-4-(2-fluorophenyl)-7,7-dimethyl-5-oxo-5,6,7,8-tetrahydro-4*H*-chromen-2-yl)formimidate (**ii-a**)

Compound **i-a** was used as the 2-amino-3-carbonitrile precursor. Pale brown solid, yield (conventional solvothermal reaction) = 0.630 g (85%), yield (using microwave-assisted reaction) = 0.648 g (88%); m.p: 205–207 °C; IR (selected ν_{max}, cm^{-1}): 2946 (C—H), 2213 (C≡N), 1612 (C=O); ^{1}H-NMR δ(ppm): 0.99 (s, 3H, CH_3), 1.06 (s, 3H, CH_3), 1.28–1.32 (t, 3H, ^{3}J = 7.1 Hz, CH_3 formimidate), 2.12–2.16 (d, 1H, ^2J = 16,2 Hz), 2.26–2.30 (d, 1H, ^2J = 16.2 Hz), 2.53–2.58 (d, 1H, ^2J = 17.9 Hz and ^2J = 17.8 Hz), 4.28-4.34 (m, 2H, CH_2 formimidate), 4.70 (s,1H, $H_{methine}$), 7.15–7.19 (m, 2H, $H_{aromatic}$), 7.26–7.33 (m, 2H, $H_{aromatic}$), 8.56 (s, 1H, N=C($H_{formimidate}$)—O); ^{13}C-NMR δ (ppm): 14.3, 27.2, 28.8, 31.7, 32.4, 50.4, 64.6, 81.3, 110.9, 115.9, 116.1, 117.5, 125.1, 125.2, 129.7, 129.9, 130.6, 156.9, 159.2, 161.7, 162.5, 164.0,

196.1; Anal. Calcd. (%) for [$C_{21}H_{21}FN_2O_3$]: C, 68.47; H, 5.75; N, 7.60; O, 13.03; found (%): C, 68.23; H, 5.73; N, 7.57; O, 12.98.

2.2.2. Ethyl (*E*)-*N*-(4-(Anthracen-9-yl)-3-cyano-7,7-dimethyl-5-oxo-5,6,7,8-tetrahydro-4*H*-chromen-2-yl)formimidate (**ii-b**)

Compound **i-b** was used as the 2-amino-3-carbonitrile precursor. Yellow solid, yield (using microwave-assisted reaction) = 0.802 g (89%), yield (using microwave-assisted reaction) = 0.838 g (93%); m.p: 192–194 °C; IR (selected ν_{max}, cm^{-1}): 2957 (C—H), 2206 (C≡N), 1604 (C=O); ^{1}H-NMR δ(ppm): 0.83 (s, 3H, CH_3), 1.05 (s, 3H, CH_3), 1.26-1.30 (t, 3H, ^3J = 7.1 Hz, CH_3 formimidate), 1.92-1.96 (d, 1H, ^2J = 16,2 Hz), 2.13-2.17 (d, 1H, ^2J = 16.2 Hz), 2.60–2.70 (overlapping doublets, 2H, ^2J = 18.0 Hz and ^2J = 18.0 Hz), 4.26–4.34 (m, 2H, CH_2 formimidate), 6.25 (s,1H, $H_{methine}$), 7.46–7.49 (m, 2H, $H_{aromatic}$), 7.54–7.62 (m, 2H, $H_{aromatic}$), 8.10–8.15 (m, 3H, $H_{aromatic}$), 8.59 (s, 1H, $H_{aromatic}$), 8.68 (s, 1H, N=C($H_{formimidate}$)—O), 8.70–8.72 (d, 1H, ^3J = 9.0 Hz, $H_{aromatic}$); ^{13}C-NMR δ (ppm): 14.2, 27.1, 28.9, 31.6, 31.9, 50.4, 64.8, 82.8, 113.4, 117.4, 123.2, 124.8, 125.1, 125.6, 126.3, 126.9, 128.6, 129.4, 129.5, 130.4, 131.3, 132.9, 156.4, 162.4, 163.4, 196.7; Anal. Calcd. (%) for [$C_{29}H_{26}N_2O_3$]: C, 77.31; H, 5.82; N, 6.22; O, 10.65; found (%): C, 77.09; H, 5.80; N, 6.20; O, 10.62.

2.2.3. Ethyl (*E*)-*N*-(3-Cyano-4-(2-fluorophenyl)-7,7-dimethyl-5-oxo-1-phenyl-1,4,5,6,7,8-hexahydroquinolin-2-yl)formimidate (**ii-c**)

Compound **i-c** was used as the 2-amino-3-carbonitrile precursor. Pale yellow solid, yield (microwave-assisted reaction) = 0.833 g (94%), yield (microwave-assisted reaction) = 0.798 g (90%); m.p: 197–199 °C; ^{1}H-NMR δ(ppm): 0.78 (s, 3H, CH_3), 0.81–0.85 (t, 3H, ^3J = 6.3 Hz, CH_3 formimidate) 0.88 (s, 3H, CH_3), 1.83–1.87 (d, 1H, ^2J = 17,5 Hz), 1.97–2.01 (d, 1H, ^2J = 16.2 Hz), 2.07 (2H, CH_2 formimidate), 2.17–2.22 (overlapping doublets, 2H, ^2J = 18.5 Hz and ^2J = 15.6 Hz), 4.89 (s,1H, $H_{methine}$), 7.14–7.22 (m, 2H, $H_{aromatic}$), 7.27–7.28 (m, 3H, $H_{aromatic}$), 7.39–7.52 (m, 4H, $H_{aromatic}$), 7.90 (s, 1H, N=C($H_{formimidate}$)—O); ^{13}C-NMR δ (ppm): 13.7, 26.6, 29.4, 31.1, 32.4, 32.9, 41.2, 49.6, 63.6, 74.2, 109.2, 115.8, 120.0, 125.2, 129.4, 129.9, 130.6, 132.2, 137.9, 152.0, 153.9, 159.1, 160.2, 161.6, 195.7; Anal. Calcd. (%) for [$C_{27}H_{26}FN_3O_2$]: C, 73.12; H, 5.91; N, 9.47; O, 7.21; found (%): C, 72.83; H, 5.89; N, 9.43; O, 7.18.

2.2.4. Ethyl (*E*)-*N*-(3-Cyano-7,7-dimethyl-5-oxo-1,4-diphenyl-1,4,5,6,7,8-hexahydroquinolin-2-yl)formimidate (**ii-d**)

Compound **i-d** was used as the 2-amino-3-carbonitrile precursor. Pale yellow solid, yield (conventional solvothermal reaction) = 0.774 g (91%), yield (microwave-assisted reaction) = 0.783 g (92%), m.p: 192–194 °C, IR (selected ν_{max}, cm^{-1}): 2965 (C—H), 2195 (C≡N), 1635 (C=O); ^{1}H-NMR δ (ppm): 0.78 (s, 3H,CH_3), 0.91 (overlapping triplet and singlet, 6H, 2CH_3), 1.87–1.91 (d,1H, ^2J = 17,45), 2.02–2.04 (d, 1H, ^2J = 16,13), 2.17–2.21 (d, 2H, ^2J = 16.60), 3.85–3.86 (q, 2H, J= 6,82), 7.35–7.38 (m, 4H, $H_{aromatic}$), 7.58–7.61 (m, 4H, $H_{aromatic}$), 8.01 (s, 1H, N=C($H_{formimidate}$)—O). ^{13}C-NMR δ (ppm): 13.5, 26.3, 29.1, 31.5, 31.8, 36.3, 49.3, 50.2, 61.3, 64.8, 110.7, 113.8, 120.0, 127.4, 129.8, 132.5, 144.7, 149.5, 151.5, 161.3, 194. 2; Anal. Calcd. (%) for [$C_{27}H_{27}N_3O_2$]: C, 76.21; H, 6.40; N, 9.87; O, 7.52; found (%): C, 75.93; H, 6.38; N, 9.83; O, 7.49.

2.2.5. Ethyl (*E*)-*N*-(1-(4-Bromophenyl)-3-cyano-7,7-dimethyl-5-oxo-4-phenyl-1,4,5,6,7,8-hexahydroquinolin-2-yl)formimidate (**ii-e**)

Compound **i-e** was used as the 2-amino-3-carbonitrile precursor. Pale yellow solid, yield (using microwave-assisted reaction) = 0.938 g (93%), yield (using microwave-assisted reaction) = 0.908 g (90%); m.p:172–174 °C, IR (selected ν_{max}, cm^{-1}): 2957 (C—H), 2196 (C≡N), 1625 (C=O); ^{1}H-NMR δ (ppm): 0.78 (s, 3H,CH_3), 0.91 (overlapping triplet and singlet, 6H, 2CH_3), 1.87–1.91 (d,1H, ^2J = 17,5 Hz), 2.02–2.04 (d, 1H, ^2J = 16,1 Hz), 2.17–2.21 (d, 2H, ^2J = 16.6 Hz), 3.85–3.86 (q, 2H, ^3J = 6,8 Hz), 7.35–7.38 (m, 4H, $H_{aromatic}$), 7.58–7.61 (m, 4H, $H_{aromatic}$), 8.01 (s, 1H, N=C($H_{formimidate}$)—O). ^{13}C-NMR δ (ppm): 13.2, 26.2, 28.9, 31.2, 37.9, 38.9, 402.2, 50.1, 61.3, 64.8, 110.7, 119.5, 121.9, 126.9, 128.9, 132.3, 136.9, 145.16,

149.9, 160.02, 194.7; Anal. Calcd. (%) for [$C_{27}H_{26}BrN_3O_2$]: C, 64.29; H, 5.20; N, 8.33; O, 6.34; found (%): C, 64.08; H, 5.18; N, 8.30; O, 6.32.

2.2.6. Ethyl (*E*)-*N*-(3-Cyano-7,7-dimethyl-5-oxo-4-phenyl-1-(p-tolyl)-1,4,5,6,7,8-hexahydroquinolin-2-yl)formimidate (**ii-f**)

Compound **i-f** was used as the 2-amino-3-carbonitrile precursor. Pale yellow solid, yield (conventional solvothermal reaction) = 0.694 g (79%), yield (microwave-assisted reaction) = 0.747 g (85%); m.p:163–165 °C, IR (selected ν_{max}, cm^{-1}): 2958 (C—H), 2193 (C≡N), 1631 (C=O); ^{1}H-NMR δ(ppm): 0.78 (s, 3H,CH_3), 0.91 (overlapping triplet and singlet, 6H, 2CH_3), 1.87–1.91 (d, 1H, ^2J = 17, 5 Hz), 1.99–2.04 (d, 1H, ^2J = 16, 1 Hz), 2.05–2.03 (d, 2H, ^2J = 16.6 Hz), 2,02 (s, 3H,CH_3) 3.85-3.86 (q, 2H, ^3J = 6,8 Hz), 7.35-7.38 (m, 4H, $H_{aromatic}$), 7.58–7.61 (m, 4H, $H_{aromatic}$), 7.96 (s, 1H, N=C($H_{formimidate}$)—O). ^{13}C-NMR δ(ppm): 13.2, 20.7, 26.3, 30.6, 31.9, 49.3, 50.1, 61.3, 79.1, 110.3, 113.9, 126.7, 127.3, 126.8, 134.9, 138.3, 145.3, 150.5, 153.2, 161.3, 194.2; Anal. Calcd. (%) for [$C_{28}H_{29}N_3O_2$]: C, 76.51; H, 6.65; N, 9.56; O, 7.28; found (%): C, 76.23; H, 6.62; N, 9.53; O, 7.25.

2.3. Crystal Structure Determination

Light yellow block-shaped crystals of **ii-b**, **ii-c** and **ii-f** that were suitable for single-crystal X-ray diffraction were obtained via hot recrystallization using ethanol. Crystal evaluation and data collection for **ii-b**, **ii-c** and **ii-f** was performed on a Bruker Smart *APEX*II (Madison, WI, USA) diffractometer with a Mo *Kα* radiation source. Reflections were collected at different starting angles, and the *APEX*II program suite was used to index the reflections [25]. Data reduction was performed using the *SAINT* [26] software, and the scaling and absorption corrections were applied using the *SADABS* [27] multi-scan technique. The structures were solved by the direct method using the *SHELXS* [28] program and refined using the *SHELXL* program [29]. Graphics of the crystal structures were drawn using *OLEX2* [30]. Non-hydrogen atoms were first refined isotropically and then by anisotropic refinement with the full-matrix least-squares method based on F^2 using *SHELXL* [29]. The disordered formimidate and 2-fluorophenyl moieties in **ii-b** and **ii-c** were modelled using PART instructions with the major components having 0.85 and 0.89 site occupancy factor, respectively. The crystallographic data and structure refinement details are summarized in Table 1.

Table 1. Crystal data and structure refinement for **ii-b**, **ii-c** and **ii-f**.

Compound	ii-b	ii-c	ii-f
Empirical formula	$C_{29}H_{26}N_2O_3$	$C_{27}H_{26}FN_3O_2$	$C_{28}H_{29}N_3O_2$
Formula weight	450.52	443.51	439.54
Temperature/K	150	100	99.99
Crystal system	Monoclinic	Monoclinic	Triclinic
Space group	$P2_1/n$	$P2_1$	P-1
a/Å	12.811(3)	9.1077(8)	9.6966(2)
b/Å	13.560(2)	24.039(2)	10.2417(2)
c/Å	14.965(3)	11.0293(10)	12.4853(2)
α/°	90	90	103.850(1)
β/°	115.110(2)	105.3140(10)	90.328(1)
γ/°	90	90	102.621(1)
Volume/Å^3	2354.0(8)	2329.0(4)	1172.57(4)
Z	4	4	2
ρ_{calc}g/cm^3	1.271	1.265	1.245
μ/mm^{-1}	0.083	0.086	0.079
F(000)	952.0	936.0	468.0
Crystal size/mm^3	0.24 × 0.16 × 0.11	0.34 × 0.26 × 0.21	0.23 × 0.18 × 0.14
2Θ range for data collection/°	4.25 to 52.256	3.388 to 54.268	4.206 to 56.9

Table 1. *Cont.*

Compound	ii-b	ii-c	ii-f
Index ranges	$-15 \leq h \leq 15$ $-16 \leq k \leq 15$ $-18 \leq l \leq 14$	$-11 \leq h \leq 10$ $-30 \leq k \leq 30$ $-14 \leq l \leq 14$	$-12 \leq h \leq 12$ $-13 \leq k \leq 13$ $-16 \leq l \leq 14$
Reflections collected	17738	34566	23267
Independent reflections	4523 R_{int} = 0.0230 R_{sigma} = 0.0225	10,085 R_{int} = 0.0166 R_{sigma} = 0.0162	5772 R_{int} = 0.0262 R_{sigma} = 0.0269
Data/restraints/parameters	4523/0/328	10085/21/610	5772/0/302
Goodness-of-fit on F^2	1.022	1.030	1.030
Final R indexes [I>=2σ (I)]	R_1 = 0.0392 wR_2 = 0.0950	R_1 = 0.0323 wR_2 = 0.0844	R_1 = 0.0432 wR_2 = 0.1090
Final R indexes [all data]	R_1 = 0.0563 wR_2 = 0.1059	R_1 = 0.0346 wR_2 = 0.0865	R_1 = 0.0570 wR_2 = 0.1171
Largest diff. peak/hole/e $Å^{-3}$	0.26/−0.16	0.38/−0.18	0.36/−0.27
Flack parameter	-	0.07(14)	-

2.4. Hirshfeld Surface Analysis

The Hirshfeld surfaces for compounds **ii-b**, **ii-c** and **ii-f**, including their respective two-dimensional fingerprint plots [31–33], were generated using *CrystalExplorer*17 [34]. All C—H bond distances were constrained to 1.083 Å when a crystallographic information file of the respective compound was read into the *CrystalExplorer*17 program [34]. The Hirshfeld surface maps generated are of a normalized contact distance, d_{norm}. This contact distance is defined in terms of the distance to the nearest atoms outside (d_e), the distance to the nearest atoms inside (d_i) [35] and the van der Waals radii [36] of the two atoms external and internal to the surface. The isovalue for the d_{norm} property of the Hirshfeld surfaces of **ii-b**, **ii-c** and **ii-f** ranged from −0.300 to 1.300.

3. Results and Discussion

3.1. Synthesis Consideration and Spectroscopic Characterization

The microwave reaction of 2-amino-3-carbonitrile derivatives (**i**), excess triethyl orthoformate and catalytic amounts of acetic acid, formed the corresponding 2-formimidate-3-carbonitriles (**ii**) as shown in Scheme 1. The short reaction time (20 min) and excellent yields (88–95%) of the desired products were obtained using this microwave radiation technique. The conventional solvothermal method also formed the desired products (**ii**) at yields that are comparable to those obtained via a microwave-assisted method in this work. However, the long reaction times are a major drawback of the conventional solvothermal method, as noted in the literature [11–23]. The ^{1}H-NMR spectra of 4H-pyran-bearing **ii** derivatives in DMSO-d_6 exhibited triplet and quartet signals at 1.3 and 4.3 ppm, which were attributed to the resonance of ethoxy protons. Furthermore, the singlet at around 8.6 ppm was attributed to the —N=C(**H**)—O— proton, which signified the formation of the formimidate backbone. Interestingly, the —N=C(**H**)—O— and ethoxy protons in the dihydropyridine-bearing **ii** derivatives are all shifted upfield with respect to those containing the 4H-pyran core. This is due to the anisotropic effect of the anilinyl ring in dihydropyridine-bearing **ii** derivatives. The IR spectra of **ii** have absorption bands at 2946–2958 cm^{-1} and 2193–2213 cm^{-1} were attributed to C—H and C≡N vibration modes, respectively. The presence of the imine functional group (C=N) was confirmed by the absorption bands at 1664–1665 cm^{-1} (in **ii-a** and **ii-b**) and 1568–1571 cm^{-1} (in **ii-c** to **ii-f**). The NMR and IR data both confirm the conversion of the NH_2 functional group in **i**, to an imine in **ii**.

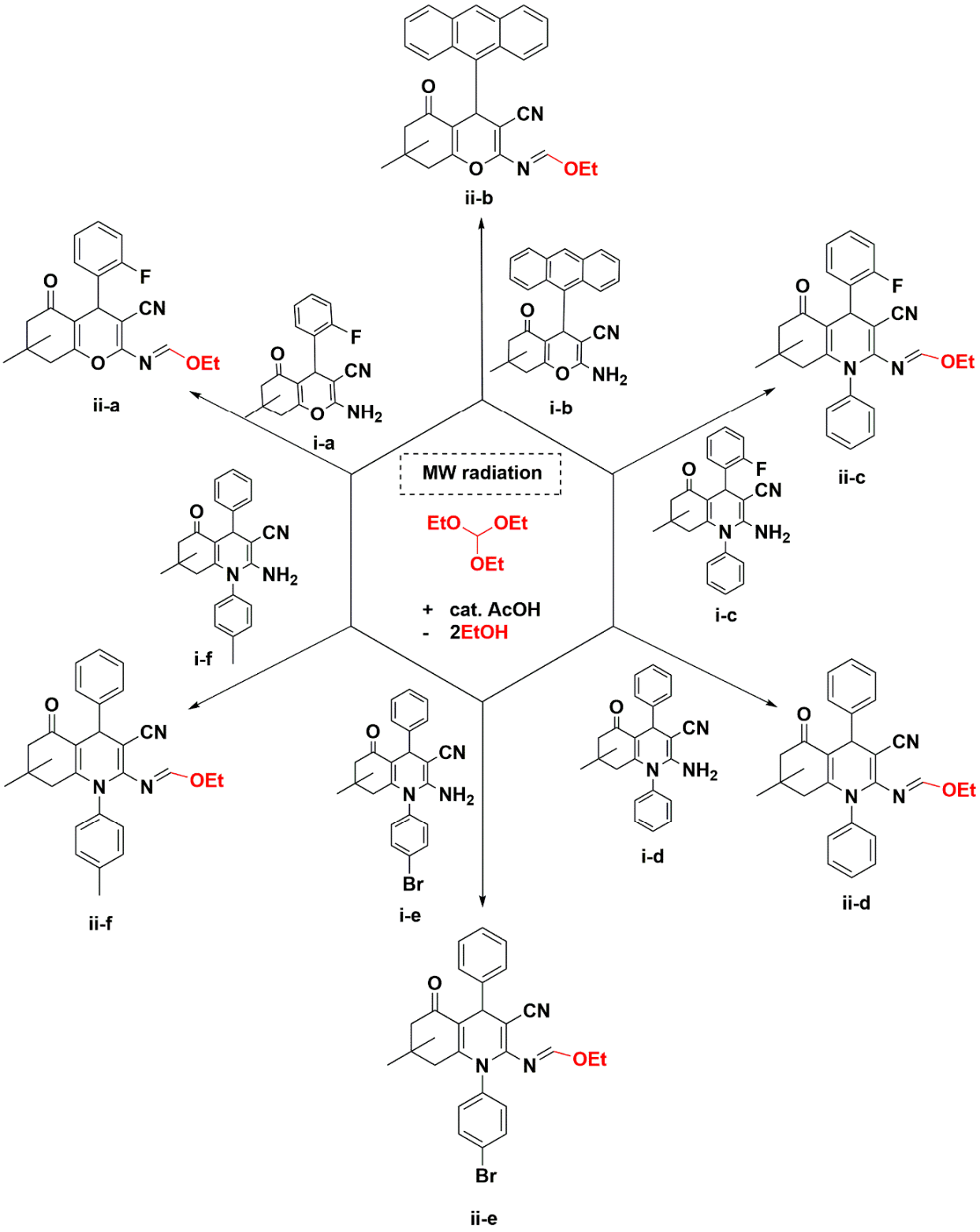

Scheme 1. Reaction scheme of 2-fomimidate-3-carbonitrile derivatives.

3.2. Crystal Structure Descriptions of **ii-b**, **ii-c** *and* **ii-f**

The crystal structures of **ii-b** and **ii-f** have one molecule in the asymmetric unit, whilst that of **ii-c** consist of two symmetrically non-equivalent molecules (Figures 1–3). In each molecule, the aryl group bonded to the C7 atom is almost orthogonal with respect to either the 4H-pyran or dihydropyridine rings. In **ii-c** and **ii-f**, the anilinyl rings were also found

to be almost perpendicular with respect to the dihydropyridine ring (C1—N1—C18—C19 torsion angle = 78.5(2)° (in **ii-c**) and 85.0(1)° (in **ii-f**)). The geometric orientation of the aryl rings is comparable to those of closely related 2-amino-3-carbonitrile in the literature [37–40]. The formimidate group in **ii-b**, **ii-c** and **ii-f** adopts an *E* configuration and is planar since the root mean squared deviation of the fitted atoms (N_{imine}=$C_{formimidate}$—O—$C_{methylene}$) ranged from 0.001 to 0.016 Å. Due to the two-part disorder in the crystal lattice in **ii-b**, near synperiplanar and synclinal conformations were observed between the formimidate group and 4H-pyran ring with $C_{formimidate}$=N_{imine}—C_{pyran}—O_{pyran} torsion angles of −12.6(2)° and 63.7(9)°, respectively. The disorder observed in ii-b can be attributed to the rotation along the C9—N1 bond. As for **ii-c** and **ii-f**, the formimidate group adopted an almost anticlinal conformation with respect to the dihydropyridine ring since the $C_{formimidate}$=N_{imine}—$C_{dihydropyridine}$—$N_{dihydropuridine}$ torsion angles were −114.2(2)−121.3(2)° and 120.5(1)°, respectively. The $C_{formimidate}$=N_{imine}—$C_{dihydropyridine}$—$N_{dihydropuridine}$ torsion angle is much wider than $C_{formimidate}$=N_{imine}—C_{pyran}—O_{pyran}, and this could be attributed to the steric demand of the anilinyl rings in **ii-c** and **ii-f**. All other intramolecular bond parameters are similar to those of previously reported compounds [11,41,42].

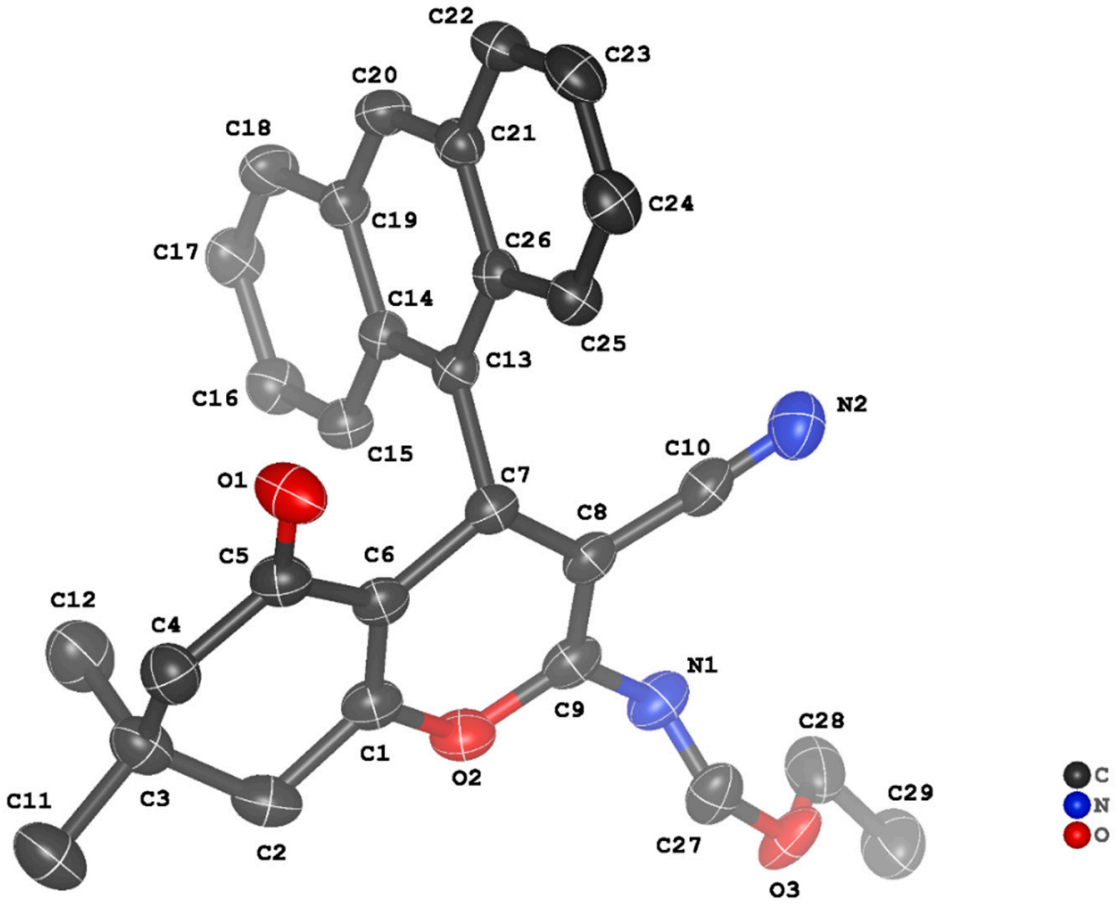

Figure 1. ORTEP diagram of **ii-b** drawn at 50% thermal ellipsoid probability. All hydrogen atoms have been omitted for clarity.

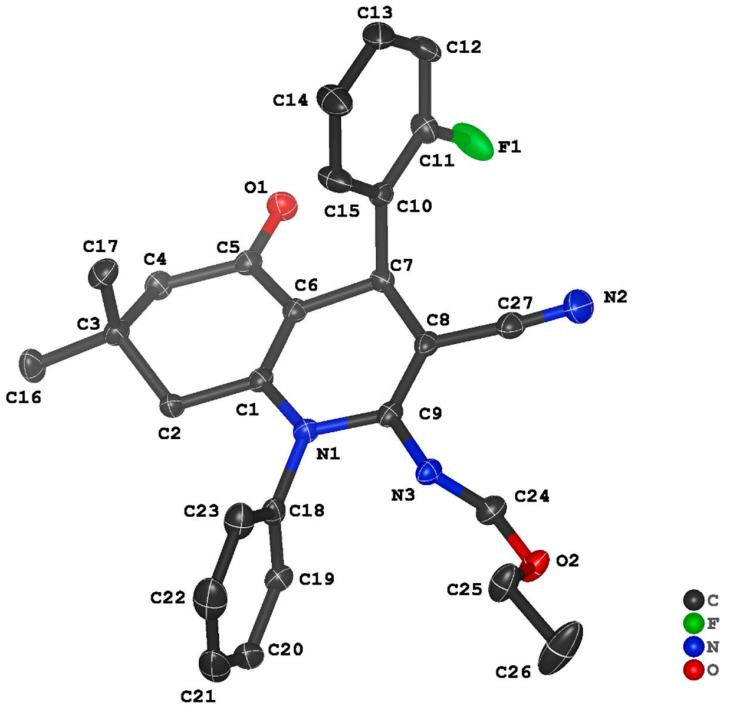

Figure 2. ORTEP diagram of **ii-c** drawn at 50% thermal ellipsoid probability. All hydrogen atoms have been omitted for clarity.

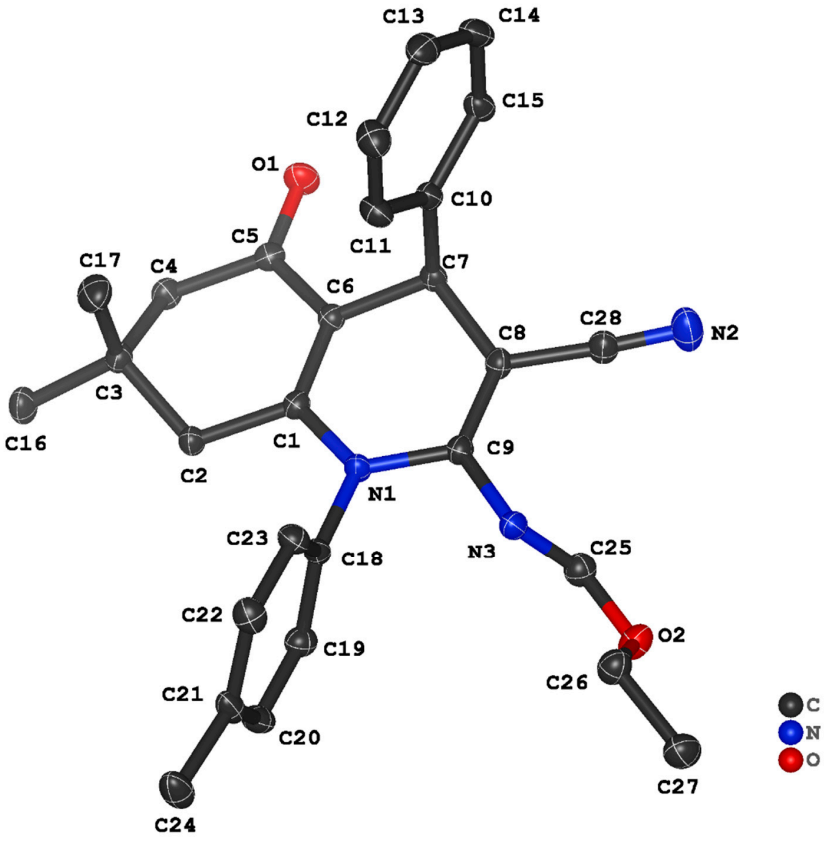

Figure 3. ORTEP diagram of **ii-f** drawn at 50% thermal ellipsoid probability. All hydrogen atoms have been omitted for clarity.

3.3. Evaluation of Intermolecular Interactions in the Crystal Packing of **ii-b**, **ii-c** *and* **ii-f**

The crystal packing of **ii-b**, **ii-c** and **ii-f** is stabilized by intermolecular hydrogen bonding interactions, which are depicted in Figures 4–6. The geometrical parameters of the various interactions are listed in Table 2. The alternating C23—H23 ... O1 and C11—H11B ... O3A hydrogen bonds in **ii-b** sew together neighbouring molecules to form chains that extend diagonally with respect to the crystallographic *a* and *c* axes (Figure 4a). These chains are further linked by C24—H24 ... N2 (Figure 4b) and C28—C28A ... $\pi_{anthracenyl}$ (Figure 5a) interactions along the crystallographic *b* axis and form a two-dimensional supramolecular structure. In **ii-c**, C12—H12 ... F2 and C39—H39 ... F1 hydrogen bonds with the $R_2^2(8)$ graphset descriptor were observed between neighbouring 2-fluorophenyl moieties (Figure 5b). Intermolecular C—H ... O were also observed in **ii-c** between the aromatic hydrogens (H19 and H50) and the carbonyl oxygen atoms (O1 and O3). The C—H ... F and C—H ... O hydrogen bonds connect neighbouring molecules form chains that extend along the crystallographic *c* axis (Figure 5b). Since the C11—H11B ... O3A and C12—H12 ... F2 hydrogen bonds include some disordered atoms (O3A in **ii-b**, F2 in **ii-c**), these intermolecular interactions are not formed in all domains of each crystal. The carbonyl oxygen (O1) in **ii-f** is involved in bifurcated C—H ... O hydrogen bonding with the aromatic H14 and H19 atoms and form chains that propagates diagonally with respect to the crystallographic *a* and *b* axes, as shown in Figure 6a. These chains are further linked together via C—H ... O hydrogen bonds between the aromatic H12 atom and O2 of the formimidate group along the crystallographic *b* axis, thus forming a two-dimensional supramolecular architecture that extends with respect to the crystallographic *ac* plane. The resultant supramolecular architecture is further stabilized by C22—H22 ... N3 and C24—H24C ... π_{phenyl} hydrogen bonds (Figure 6b).

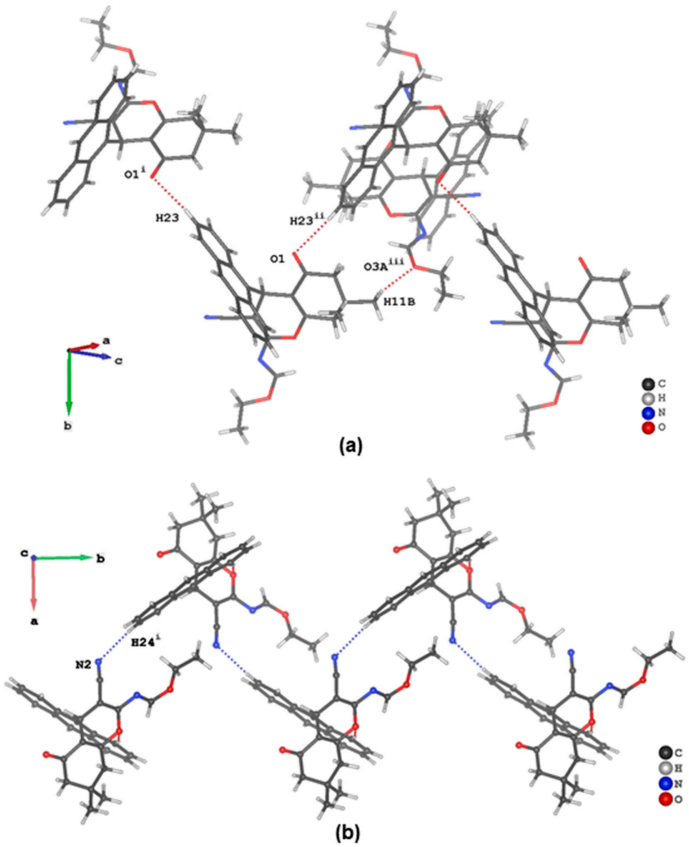

Figure 4. Representation of intermolecular (**a**) C—H ... O and (**b**) C—H ... N hydrogen bonds in the crystal packing of **ii-b**. C—H ... O and C—H ... N hydrogen bonds are shown as red- and blue-dotted bonds, respectively.

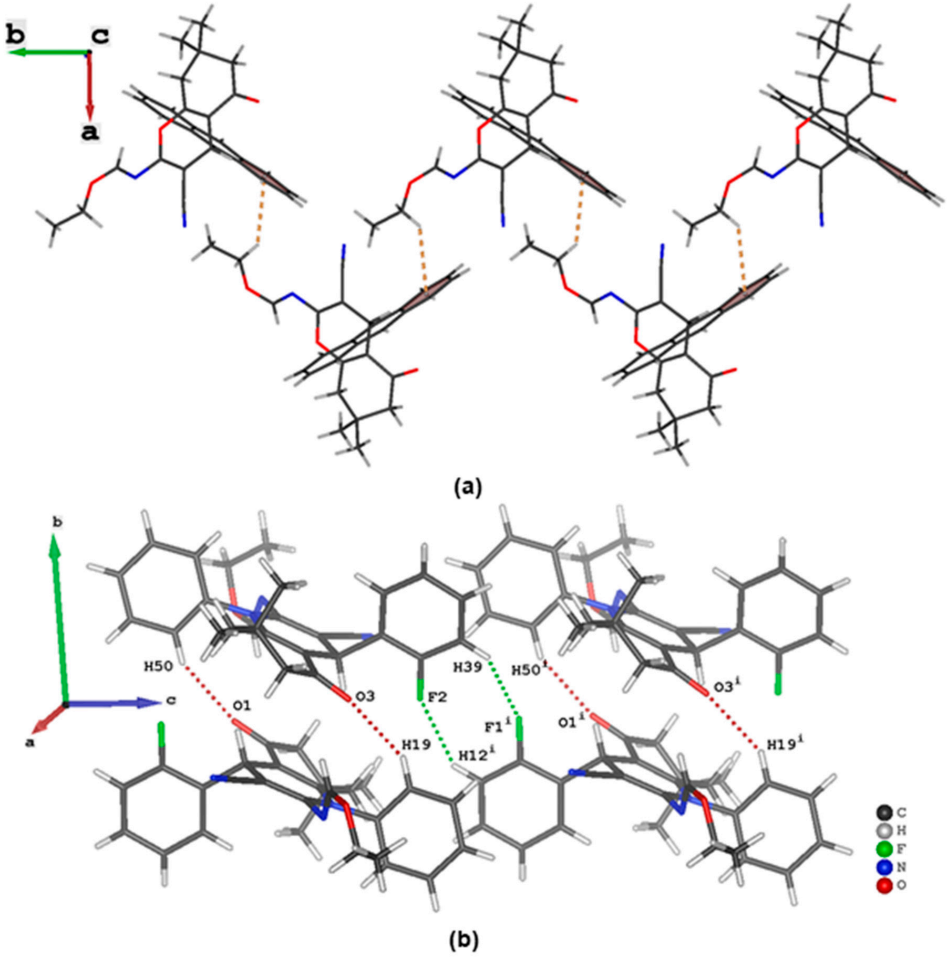

Figure 5. Representation of intermolecular (**a**) C28—H28A ... $\pi_{anthracenyl}$ (**b**) C—H ... O and C—H ... F hydrogen bonds in the crystal packing of **ii-b** and **ii-c**, respectively. C—H ... $\pi_{anthracenyl}$, C—H ... O and C—H ... F hydrogen bonds are shown as orange-, red- and green-dotted bonds, respectively.

Table 2. Selected hydrogen bonds for **ii-b**, **ii-c** and **ii-f**.

D	H	A	d(D-H)/Å	d(H ... A)/Å	d(D ... A)/Å	D-H ... A/°
			Compound **ii-b**			
C11	H11C	O3A ^{i}	0.98	2.66	3.481(3)	142
C15	H15	O2	0.95	2.62	3.559(2)	168
C23	H23	O1 ^{ii}	0.95	2.57	3.487(2)	164
C24	H24	N2 ^{iii}	0.95	2.63	3.574(2)	170
C28	H28A	$\pi_{anthracenyl}$ ^{iv}	0.98	2.92	3.692(2)	136
			Compound **ii-c**			
C12	H12	F2 ^{i}	0.95	2.58	3.361(3)	140
C19	H19	O3	0.95	2.56	3.396(3)	147
C50	H50	O1	0.95	2.52	3.371(3)	149
			Compound **ii-f**			
C19	H19	O1 ^{i}	0.95	2.52	3.440(2)	163
C12	H12	O2 ^{ii}	0.95	2.65	3.469(2)	145
C14	H14	O1 ^{iii}	0.95	2.55	3.484(2)	170
C22	H22	N3 ^{iv}	0.95	2.66	3.351(2)	131
C24	H24C	π_{phenyl} ^{iv}	0.98	2.66	3.558(2)	152

Symmetry codes for **ii-b**: (i) 1/2- *x*,-1/2+ *y*,5/2- *z*; (ii) -1/2+ *x*,1/2- *y*,-1/2+ *z*; (iii) -1/2- *x*,-1/2+ *y*,3/2- *z*; (iv) -*x*,1- *y*,2- *z*; for **ii-c**: (i) *x*,+*y*,-1+ *z*; for **ii-f**: (i) 1- *x*,2- *y*,-*z*; (ii) *x*,-1+ *y*,+ *z*; (iii) -*x*,1- *y*,-*z*; (iv) 1- *x*,2- *y*,1- *z*.

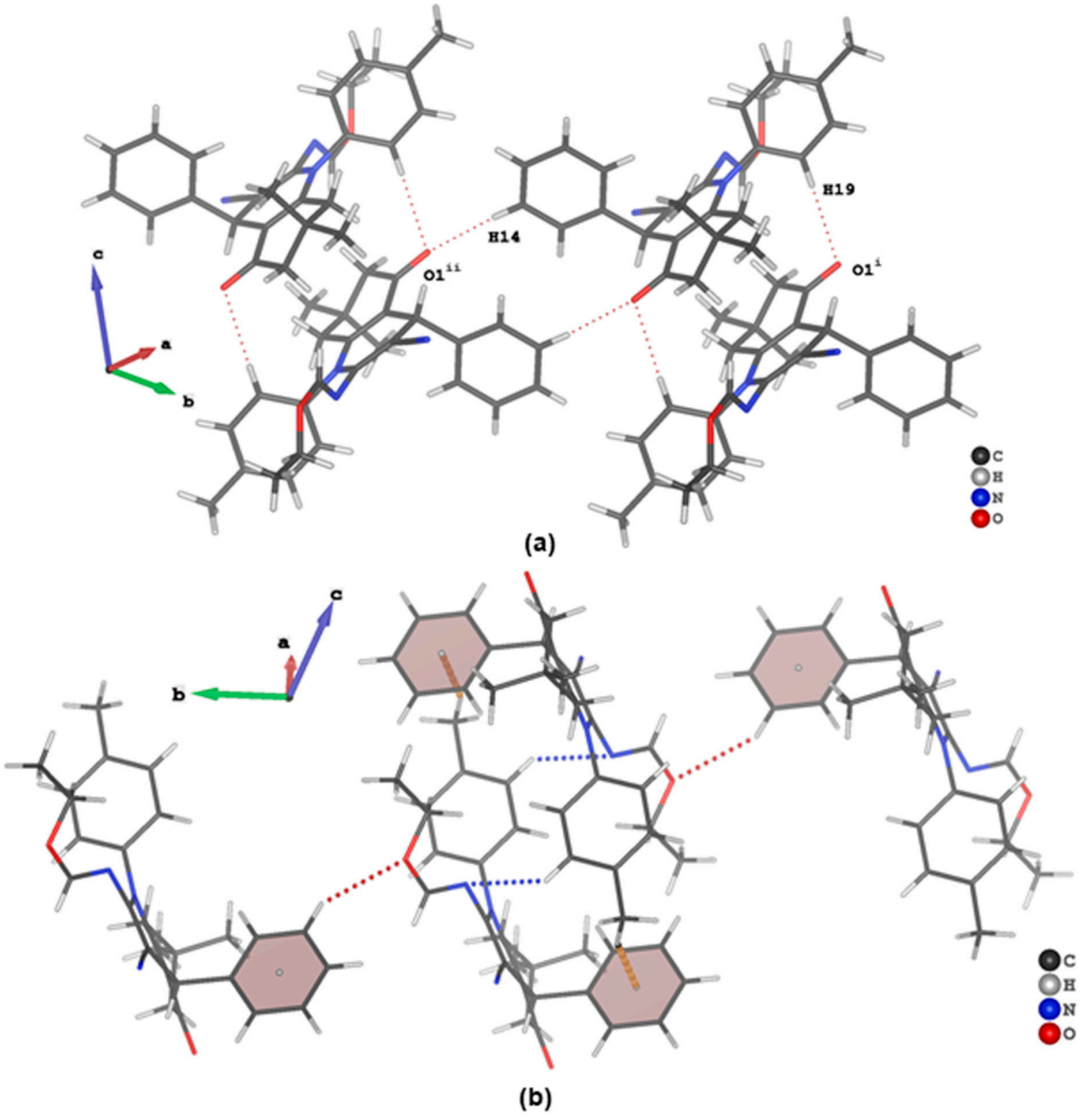

Figure 6. Representation of intermolecular (**a**) C—H . . . O, (**b**) C12—H12 . . . O2, C22—H22 . . . N3 and C24—H24C . . . π_{phenyl} hydrogen bonds in the crystal packing of **ii-f**. C—H . . . O, C—H . . . N and C—H . . . π hydrogen bonds are shown as red-, blue- and orange-dotted bonds, respectively.

3.4. CSD Survey of Closely Related Compounds

To put our work into some perspective, a survey of the Cambridge Structural Database (CSD; version 5.42, September 2021 update) [43] was conducted. Figure 7 shows the three hits that were obtained for closely related 2-formimidate-3-carbonitrle derivatives bearing a 4H-pyran moiety (CSD refcodes: **BEPZAZ**, **GINZOT** and **ZAQFUV**). The aryl rings bonded to the stereogenic centre in the three hits have a similar geometric orientation to those observed in **ii-b**, **ii-c** and **ii-f**. The formimidate functional group is almost *syn*-periplanar with the 4H-pyran ring in **BEPZAZ**, **GINZOT** and **ZAQFUV** since the $C_{formimidate}$=N_{imine}—C_{pyran}—O_{pyran} torsion angle was found to be 1.7(2)°, 8.0(2)° and 3.7(3)°, respectively. No crystal structure of 2-formimidate-3-carbonitrle derivatives bearing a dihydropyridine moiety exists on the CSD. Thus, the first CSD entry of crystal structures of such derivatives is reported in this work. Interestingly, the formimidate group seems to prefer to adopt an *E* configuration in the solid state despite the variation in the groups on the 4H-pyran or dihydropyridine core.

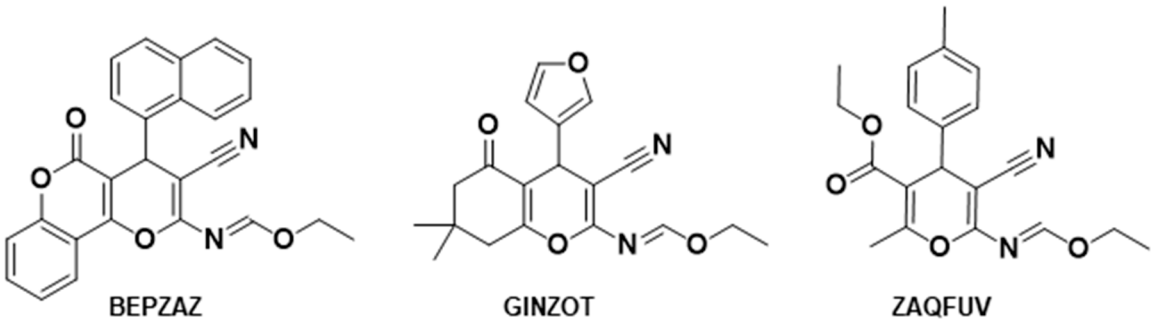

Figure 7. Hits from the CSD survey.

3.5. Hirshfeld Surface Analysis

Hirshfeld surface analysis was used to examine the contribution of the various intermolecular interactions observed in **ii-b**, **ii-c** and **ii-f** towards the stabilization of the crystal lattice. This was achieved by generating d_{norm} Hirschfeld surfaces and two-dimensional fingerprint plots as depicted in Figure 8. The red regions on the d_{norm} surface signify close intermolecular contacts attributed to the various hydrogen bonds discussed. The white regions on the d_{norm} surface indicate van der Waals contacts whilst the blue regions signify very weak intermolecular contacts. In all three compounds, the H . . . H contacts contribute the most towards (50.2–58.6%) the Hirshfeld surface. The reciprocal H..C contacts were attributed to C—H . . . π interactions, and they constitute 14.3–23.9% of the Hirshfeld surface. Compound **ii-b** had the highest contribution of H . . . C/C . . . H contacts, and this could be attributed to the presence of more aromatic rings than in **ii-c** and **ii-f.** The lowest contribution of reciprocal C . . . H contacts was observed in **ii-c**, and this deficit was attributed to the presence of C—H . . . F hydrogen bonds with reciprocal H . . . F contact contributions of 9.4%. There seems to be no significant difference in the contribution of N . . . H/H . . . N contacts across all three compounds. This is probably due to the very weak intermolecular van der Waals forces in N . . . H contacts. The reciprocal O . . . H contacts were attributed to intermolecular C—H . . . O hydrogen bonds, and the lowest contribution was observed in **ii-c** (9.6%) due to the existence of C—H . . . F hydrogen bonds. This deficit is further compounded by the low number of oxygen atoms in **ii-c** as compared to that in **ii-a** and **ii-f**.

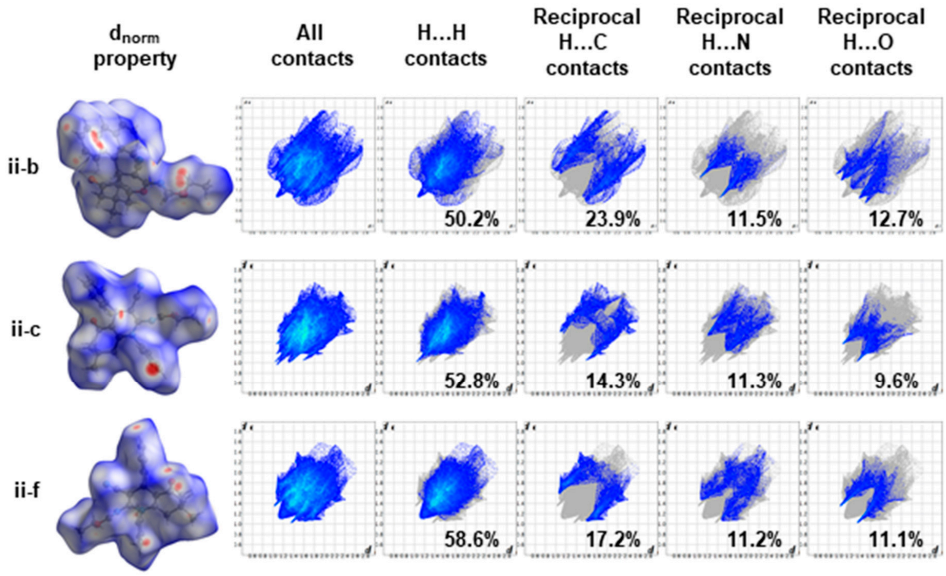

Figure 8. The d_{norm} property mapped over the Hirshfeld surfaces and selected two-dimensional fingerprint plots with their respective contributions of **ii-b**, **ii-c** and **ii-f**.

4. Conclusions

The formation of 2-formimidate-3-carbonitrile derivatives via microwave reactions of triethyl orthoformate with corresponding 4H-pyran- and dihydropyridine-based 2-amino-3-carbonitrile precursors was successful. In comparison to the conventional synthesis protocol, the use of microwave radiation significantly reduced the reaction times from the order of hours to 20 min whilst maintaining the reaction yields. The synthesis of the desired products was confirmed using NMR and IR spectroscopy. In the solid state, the formimidate functional group adopts an *E* configuration based on the single-crystal X-ray diffraction. The 4H-pyran-based derivatives adopt *syn*-periplanar and synclinal conformations between the formimidate group and pyran ring whilst an anticlinal conformation was observed for dihydropyridine-based derivatives. The crystal lattices of 2-formimidate-3-carbonitrile derivatives in this work are stabilized by classical but weak intermolecular hydrogen bonds, which include C—H ... O, C—H ... N, C—H ... F (in **ii-c**) and C—H ... π. According to the Hirshfeld surface analysis, the 2-formimidate-3-carbonitrile derivative bearing 4H-pyran (**ii-b**) has larger contributions of C—H ... π and C—H ... O hydrogen bonds towards the Hirshfeld surface than those of the dihydropyridine-based derivatives (**ii-c** and **ii-f**). This was attributed to the presence of anthracenyl and 4H-pyran moieties in **ii-b**. However, the contribution of reciprocal H ... N contacts towards the Hirshfeld surface seems to be independent of the nature of the central ring (4H-pyran or dihydropyridine) and the substituents on it. We are currently investigating the preferred isomerism of 2-formimidate-3-carbonitrile derivatives in solution state. These findings could provide better insight into how the choice of solvent and reaction conditions play a key role in the formation of fused pyrimidines.

Supplementary Materials: The following are available online. Figures S1–S12: 1H- and 13C-NMR spectra of ii-a to ii-f, Figures S13–S17: IR spectra of **ii-a** to **ii-f**.

Author Contributions: Conceptualization, S.J.Z. and B.O.; methodology, S.J.Z.; formal analysis, S.J.Z.; investigation, S.J.Z.; data curation, S.J.Z.; writing—original draft preparation, S.J.Z.; writing—review and editing, B.O.; supervision, B.O.; project administration, B.O. All authors have read and agreed to the published version of the manuscript.

Funding: This work and the APC was funded by the University of KwaZulu-Natal.

Institutional Review Board Statement: Not applicable.

Informed Consent Statement: Not applicable.

Data Availability Statement: Crystallographic data for the structures have been deposited with the Cambridge Crystallographic Data Centre (CCDC no. 2169894-2169896). Copies of this information may be obtained free of charge from The Director, CCDC, 12 Union Road, Cambridge, CB2 1EZ, UK (fax: +44-1223-336033; email: deposit@ccdc.cam.ac.uk or http://www.ccdc.cam.ac.uk (accessed on 16 March 2022)).

Conflicts of Interest: The authors declare no conflict of interest.

References

1. Haggam, R.A.; Assy, M.G.; Mohamed, E.K.; Mohamed, A.S. Synthesis of Pyrano[2,3-d]pyrimidine-2,4-diones and Pyridino[2,3-d]pyrimidine-2,4,6,8-tetraones: Evaluation Antitumor Activity. *J. Heterocycl. Chem.* **2020**, *57*, 842–850. [CrossRef]
2. Suresh, L.; Kumar, P.S.V.; Chandramouli, G.V.P. An efficient one-pot synthesis, characterization and antibacterial activity of novel chromeno-pyrimidine derivatives. *J. Mol. Struct.* **2017**, *1134*, 51–58. [CrossRef]
3. Belhadj, F.; Kibou, Z.; Benabdallah, M.; Aissaoui, M.; Rahmoun, M.N.; Villemin, D.; Choukchou-Braham, N. Synthesis and Biological Evaluation of New Chromenes and Chromeno[2,3-d] pyrimidines. *S. Afr. J. Chem.* **2021**, *75*, 150–155. [CrossRef]
4. El-Sayed, R.; Fadda, A.A. Synthesis of Pharmacological Heterocyclic Derivatives Based Surfactants. *J. Oleo Sci.* **2016**, *65*, 929–940. [CrossRef] [PubMed]
5. Abu El-Azm, F.S.M.; El-Shahawi, M.M.; Elgubbi, A.S.; Madkour, H.M.F. Design, synthesis, anti-proliferative activity, and molecular docking studies of novel benzo[f]chromene, chromeno [2,3-d]pyrimidines and chromenotriazolo[1,5-c]pyrimidines. *Synth. Commun.* **2020**, *50*, 669–683. [CrossRef]

6. Halawa, A.H.; Elaasser, M.M.; El Kerdawy, A.M.; Abd El-Hady, A.M.A.I.; Emam, H.A.; El-Agrody, A.M. Anticancer activities, molecular docking and structure–activity relationship of novel synthesized 4H-chromene, and 5H-chromeno[2,3-d]pyrimidine candidates. *Med. Chem. Res.* **2017**, *26*, 2624–2638. [CrossRef]
7. Bassyouni, F.; Tarek, M.; Salama, A.; Ibrahim, B.; Salah El Dine, S.; Yassin, N.; Hassanein, A.; Moharam, M.; Abdel-Rehim, M. Promising Antidiabetic and Antimicrobial Agents Based on Fused Pyrimidine Derivatives: Molecular Modeling and Biological Evaluation with Histopathological Effect. *Molecules* **2021**, *26*, 2370. [CrossRef]
8. Gouhar, R.; Abou-Elmagd, W.; El-Zahar, M.; Kamel, M.; El-Ghonamy, D. Synthesis of novel 5,6,7,8,9,10-hexahydropyrimido[4,5-b]quinoline derivatives for antimicrobial and anti-oxidant evaluation. *Res. Chem. Intermed.* **2017**, *43*, 1301–1327. [CrossRef]
9. Taylor, E.C.; Ehrhart, W.A. A Convenient Synthesis of N,N′-Disubstituted Formamidines and Acetamidines1. *J. Org. Chem.* **1963**, *28*, 1108–1112. [CrossRef]
10. Yoon, D.S.; Han, Y.; Stark, T.M.; Haber, J.C.; Gregg, B.T.; Stankovich, S.B. Efficient Synthesis of 4-Aminoquinazoline and Thieno[3,2-d]pyrimidin-4-ylamine Derivatives by Microwave Irradiation. *Org. Lett.* **2004**, *6*, 4775–4778. [CrossRef]
11. Abdelrazek, F.M.; Metz, P.; Kataeva, O.; Jaeger, A.; El-Mahrouky, S.F. Synthesis and molluscicidal activity of new chromene and pyrano[2,3-c]pyrazole derivatives. *Arch. Pharm.* **2007**, *340*, 543–548. [CrossRef]
12. Ameli, S.; Davoodnia, A.; Pordel, M.; Behmadi, H. Synthesis of New Imino Containing Tetrahydrochromeno[2,3-d]pyrimidines. *J. Heterocycl. Chem.* **2017**, *54*, 1437–1441. [CrossRef]
13. Debbabi, M.; Nimbarte, V.D.; Chekir, S.; Chortani, S.; Romdhane, A.; Ben Jannet, H. Design and synthesis of novel potent anticoagulant and anti-tyrosinase pyranopyrimidines and pyranotriazolopyrimidines: Insights from molecular docking and SAR analysis. *Bioorganic Chem.* **2019**, *82*, 129–138. [CrossRef] [PubMed]
14. Erichsen, M.N.; Huynh, T.H.V.; Abrahamsen, B.; Bastlund, J.F.; Bundgaard, C.; Monrad, O.; Bekker-Jensen, A.; Nielsen, C.W.; Frydenvang, K.; Jensen, A.A.; et al. Structure-Activity Relationship Study of First Selective Inhibitor of Excitatory Amino Acid Transporter Subtype 1: 2-Amino-4-(4-methoxyphenyl)-7-(naphthalen-1-yl)-5-oxo-5,6,7,8-tetrahydro-4H-chromene-3-carbonitrile (UCPH-101). *J. Med. Chem.* **2010**, *53*, 7180–7191. [CrossRef] [PubMed]
15. Fadda, A.A.; Youssif, E.H.E. Synthesis of Some New Chromene Derivatives, Part 6. *Synth. Commun.* **2011**, *41*, 677–694. [CrossRef]
16. Hassanien, A.A.; Zahran, M.A.; El-Gaby, M.S.A.; Ghorab, M.M. Utility of 2-amino-4,5,6,8-tetrahydro-7H-chromene-3-carbonitriles in synthesis of chromeno[2,3-d]pyrimidine and chromeno[3,2-e][1,2,4]triazolo[1,5-c]pyrimidine derivatives of pharmaceutical interest. *J. Indian Chem. Soc.* **1999**, *76*, 350–354. [CrossRef]
17. Hu, J.-L.; Sha, F.; Li, Q.; Wu, X.-Y. Highly enantioselective Michael/cyclization tandem reaction between dimedone and isatylidene malononitriles. *Tetrahedron* **2018**, *74*, 7148–7155. [CrossRef]
18. Kong, X.-X.; Cao, Y.-N.; Xing, Z.; Chen, L.-Z.; Han, G.-F. Synthesis of novel 15-aryl-2,3,4,15-tetrahydrochromeno[2′,3′:4,5]pyrimido quinazoline-1,9-diones. *J. Chem. Res.* **2016**, *40*, 87–91. [CrossRef]
19. Li, B.; Wang, Z.-X.; Xing, Z.; Chen, L.-Z.; Han, G.-F. Synthesis of novel 2-methyl and 2-cyanomethyl-12-aryl-8,12-dihydro-9H-chromeno[3,2-e][1,2,4]triazolo[1,5-c]pyrimidin-11(10H)-one derivatives. *J. Chem. Res.* **2015**, *39*, 30–35. [CrossRef]
20. Mahdavi, S.M.; Habibi, A.; Dolati, H.; Shahcheragh, S.M.; Sardari, S.; Azerang, P. Synthesis and antimicrobial evaluation of 4H-pyrans and Schiff bases fused 4H-pyran derivatives as inhibitors of Mycobacterium bovis (BCG). *Iran. J. Pharm. Res.* **2018**, *17*, 1229–1239.
21. Mobinikhaledi, A.; Foroughifar, N.; Mosleh, T.; Hamta, A. Synthesis of some novel chromenopyrimidine derivatives and evaluation of their biological activities. *Iran. J. Pharm. Res.* **2014**, *13*, 873–879. [PubMed]
22. Wang, Z.-X.; Li, B.; Xing, Z.; Chen, L.-Z.; Han, G.-F. Synthesis of novel 9,9-dimethyl-8,12-dihydro-9H-chromeno[3,2-e][1,2,4] triazolo[1,5-c]pyrimidin-11(10H)-one derivatives. *J. Chem. Res.* **2014**, *38*, 480–485. [CrossRef]
23. Youssef, M.S.K.; Abeed, A.A.O.; El-Emary, T.I. Synthesis and evaluation of chromene-based compounds containing pyrazole moiety as antimicrobial agents. *Heterocycl. Commun.* **2017**, *23*, 55–64. [CrossRef]
24. Singh, S.K.; Singh, K.N. DBU-catalyzed expeditious and facile multicomponent synthesis of N-arylquinolines under microwave irradiation. *Mon. Chem.* **2012**, *143*, 805–808. [CrossRef]
25. Bruker. *APEXII*; Bruker AXS: Madison, WI, USA, 2009.
26. Bruker. *SAINT*; Bruker AXS: Madison, WI, USA, 2009.
27. Bruker. *SADABS*; Bruker AXS: Madison, WI, USA, 2009.
28. Sheldrick, G.M. A short history of SHELX. *Acta Crystallogr. Sect. A Found. Crystallogr.* **2008**, *64*, 112–122. [CrossRef] [PubMed]
29. Sheldrick, G.M. Crystal structure refinement with SHELXL. *Acta Crystallogr. Sect. C Struct. Chem.* **2015**, *71*, 3–8. [CrossRef]
30. Dolomanov, O.V.; Bourhis, L.J.; Gildea, R.J.; Howard, J.A.; Puschmann, H. OLEX2: A complete structure solution, refinement and analysis program. *J. Appl. Crystallogr.* **2009**, *42*, 339–341. [CrossRef]
31. Hirshfeld, F.L. Bonded-atom fragments for describing molecular charge densities. *Theor. Chim. Acta* **1977**, *44*, 129–138. [CrossRef]
32. Spackman, M.A.; Jayatilaka, D. Hirshfeld surface analysis. *Cryst. Eng. Commun.* **2009**, *11*, 19–32. [CrossRef]
33. Spackman, M.A.; McKinnon, J.J. Fingerprinting intermolecular interactions in molecular crystals. *Cryst. Eng. Commun.* **2002**, *4*, 378–392. [CrossRef]
34. Turner, M.; McKinnon, J.; Wolff, S.; Grimwood, D.; Spackman, P.; Jayatilaka, D.; Spackman, M. *CrystalExplorer17*; The University of Western Australia: Perth, Australia, 2017.
35. McKinnon, J.J.; Jayatilaka, D.; Spackman, M.A. Towards quantitative analysis of intermolecular interactions with Hirshfeld surfaces. *Chem. Commun.* **2007**, 3814–3816. [CrossRef] [PubMed]

36. Bondi, A. Van der Waals volumes and radii of metals in covalent compounds. *J. Phys. Chem.* **1966**, *70*, 3006–3007. [CrossRef]
37. Zanin, L.L.; Jimenez, D.E.Q.; de Jesus, M.P.; Diniz, L.F.; Ellena, J.; Porto, A.L.M. Synthesis and X-ray crystal structures of polyfunctionalized 4H-chromene derivatives via tricomponent reaction with Knoevenagel adducts as intermediates in aqueous medium. *J. Mol. Struct.* **2021**, *1223*, 129226. [CrossRef]
38. Ramesh, R.; Maheswari, S.; Malecki, J.G.; Lalitha, A. NaN_3 Catalyzed Highly Convenient Access to Functionalized 4H-chromenes: A Green One-pot Approach for Diversity Amplification. *Polycycl. Aromat. Compd.* **2020**, *40*, 1581–1594. [CrossRef]
39. Maharramov, A.; Kaya, R.; Taslimi, P.; Kurbanova, M.; Sadigova, A.; Farzaliyev, V.; Sujayev, A.; Gulçin, İ. Synthesis, crystal structure, and biological evaluation of optically active 2-amino-4-aryl-7,7-dimethyl-5-oxo-5,6,7,8-tetrahydro-4H-chromen-3-carbonitriles: Antiepileptic, antidiabetic, and anticholinergics potentials. *Arch. Pharm.* **2019**, *352*, 1800317. [CrossRef]
40. Jiang, H.; Wang, X.-S.; Zhang, M.-M.; Li, Y.-L.; Shi, D.-Q. 2-Amino-4-(2-chlorophenyl)-7,7-dimethyl-1-(4-methylphenyl)-5-oxo-1,4,5,6,7,8-hexahydroquinoline-3-carbonitrile. *Acta Crystallogr. Sect. E* **2006**, *62*, o1184–o1186. [CrossRef]
41. Al-Masoudi, N.A.; Mohammed, H.H.; Hamdy, A.M.; Akrawi, O.A.; Eleya, N.; Spannenberg, A.; Pannecouque, C.; Langer, P. Synthesis and anti-HIV Activity of New Fused Chromene Derivatives Derived from 2-Amino-4-(1-naphthyl)-5-oxo-4H,5H-pyrano[3,2- c]chromene-3-carbonitrile. *Z. Nat. B* **2013**, *68*, 229–238. [CrossRef]
42. Shi, Q.-Z.; Cao, Y.-N.; Ma, S.-B.; Wang, G.-X.; Han, G.-F.; Xing, Z. Synthesis of Novel Ethyl 1-aryl-3-methyl-8-oxo-1,8-dihydropyrano[2′,3′:4,5] Pyrimido[6,1-b]Quinazoline-2-carboxylate Derivatives. *J. Chem. Res.* **2016**, *40*, 767–771. [CrossRef]
43. Groom, C.R.; Bruno, I.J.; Lightfoot, M.P.; Ward, S.C. The Cambridge Structural Database. *Acta Crystallogr. Sect. B Struct. Sci. Cryst. Eng. Mater.* **2016**, *72*, 171–179. [CrossRef]